# Temperature imaging in low pressure flames using diode laser two-line atomic fluorescence employing a novel indium seeding technique

Jesper Borggren[1], Iain S. Burns[2], Anna-Lena Sahlberg[1], Marcus Aldén[1] and Zhongshan Li[1]

[1]Division of Combustion Physics, Lund University, P.O. Box 118, S221 00 Lund, Sweden
[2]Department of Chemical and Process Engineering, University of Strathclyde, Glasgow G1 1XJ, Scotland, United Kingdom

## *Abstract*

The use of diode lasers for spatially resolved temperature imaging is demonstrated in low pressure premixed methane-air flames using two-line atomic fluorescence of seeded indium atoms. This work features the advantages of using compact diode lasers as the excitation sources with the benefits of two-dimensional planar imaging, which is normally only performed with high-power pulsed lasers. A versatile and reliable seeding technique with minimal impact on flame properties is used to introduce indium atoms into the combustion environment for a wide range of flame equivalence ratios. A spatial resolution of around 210 µm for this calibration free thermometry technique is achieved for three equivalence ratios at a pressure of 50 mbar in a laminar flat flame.

Key words: TMIn seeding, two-line atomic fluorescence, temperature, low pressure flame, diode lasers, imaging

## *1. Introduction*

The temperature in thermochemical processes, such as combustion, is one of the major governing physical properties due to the strong relation between temperature and reaction rates. Chemical kinetic models striving to understand, explain and model the combustion process are highly dependent on accurate experimental data for validation and optimization, where temperature information is a crucial parameter. For the development of kinetic models low pressure flat flames are frequently used due to the advantage of a thickened reaction zone and the one dimensional nature of the flame [1, 2]. Most of the flame temperature measurements in low pressure laminar flames for kinetic development still employ intrusive methods, predominantly thermocouples [3, 4]. Although of great interest, non-intrusive temperature measurements in low pressure flames have been rather rarely implemented and even less so techniques with imaging capabilities. Thus, a technique combining the advantages of planar imaging thermometry with the use of low-power diode laser sources would offer distinct advantages over present techniques.

The reduced volume number density in low pressure flames limits the use of many techniques applicable at atmospheric pressures, e.g. scattering techniques such as Rayleigh and Raman scattering. Rayleigh thermometry [5] in low pressure flames is also vulnerable to elastically scattered light from the low pressure chamber. Low signal-to-noise ratio (SNR) has also be reported for Stokes/anti-Stokes Raman measurements of $H_2$, CO and $H_2O$ conducted in fuel-rich low pressure flames preventing accurate temperature measurements at pressures below 200 mbar [6], while also restricted to point measurements or at most along a line.

Hartlieb et al. [6] investigated the feasibility of single-point temperature measurements based on multi-line laser-induced fluorescence of naturally occurring OH and seeded NO,

where calculated spectral line intensities are fitted to a recorded rotational spectrum to extract information of temperature. Low concentration of OH, especially in rich flames, limits the region that can be investigated with OH thermometry. The technique also suffers from having to compensate for the rotational-line dependence of quenching cross-sections to the fluorescence quantum yield. Multi-line NO LIF based on a high-power tunable excimer laser has also been used for 2D temperature imaging in low pressure nano-particle synthesis flames offering a temperature range between 600-1500 K [7]. A substantial amount of NO has to be seeded into the gas flow to achieve a decent signal-to-noise ratio, which may have non-negligible effects on the flame chemistry.

With the recent advances in hybrid femto/picosecond coherent anti-stokes Raman spectroscopy (CARS) the technique previously limited to point measurements have been expanded to 1D and even 2D measurements at atmospheric pressures [8, 9]. CARS is, however, expected to have decreased usability in low pressure environments as the signal is proportional to the square of the number density. Even so, measurements in low pressure hydrogen flames have been reported successful [10]. The CARS technique also suffers from an experimentally complicated setup involving expensive and bulky equipment.

Absorption based techniques benefit from experimental simplicity and straight-forward data evaluation and numerous papers present temperature measurements utilizing absorption techniques either based on near infrared diode lasers or quantum cascade lasers [11, 12]. Commonly a tunable diode laser is scanned over either one or a few well-known absorption lines. For the two line approach the lines are usually chosen so the ratio of the intensity of two lines is temperature sensitive and the temperature can be extracted if the line-strengths are well-known. A one-line method can also be used where a recorded line-shape is fitted and the Doppler broadening due to thermal molecular motion is calculated. Absorption based

techniques are limited to path-integrated temperatures along the line-of-sight and even in one dimensional flames, edge effects may contribute to errors in measured temperatures, although this can be minimised with the proper precautions [11].

With the introduction of laser diodes in the blue wavelength region temperature measurements using atomic fluorescence of indium have been reported, both a two-line method [13, 14] and a one-line scanning method, termed OLAF, [15]. Both methods will be described in detail in the next section. The two line method is especially suitable for sooty and particle laden flames as elastic scattering can be filtered. However, even detection of resonant fluorescence have been shown to work well for low pressure sooty flames [13] due to the high quantum yield of the atomic fluorescence. In these papers indium was seeded into the flame using $InCl_3$ dissolved in water. The introduction of a few percent water vapour will potentially influence the flame chemistry and a temperature uncertainty of ±20 K has been estimated to be caused from this seeding method [16]. Previous work has been limited to point measurements due to weak powers of the diode lasers and mapping of the flame temperature have been a somewhat time consuming process. As evident, there is still room for developing a diagnostic method that can image the temperature with good accuracy and spatial resolution using diode lasers.

In this work we present the development of a temperature imaging technique with diode lasers using two-line atomic fluorescence in low pressure flames. Imaging is possible due to the development of higher power diode lasers in combination with a state-of-the-art intensified high speed camera, working in the linear regime. A novel indium seeding system, previously described [16], with negligible impact on flame properties is used to access temperature information from the reaction zone to the product zone for a wide variety of equivalence ratios at pressures of 50 mbar. The seeding system also allows for seeding

through sintered porous plug burners commonly employed in low pressure flame studies for kinetic modelling [17] and the temperature measurements conducted here are included in a larger effort striving to perform accurate quantitative measurements of species concentrations in low pressure flames using infra-red polarization spectroscopy (IRPS) for model validation and kinetic simulations [18, 19].

The theory of two-line atomic fluorescence method is explained and temperature measurements for different equivalence ratios are presented. The demonstrated technique is shown to be a valuable tool for temperature measurements that can be expanded into sooty flames and higher pressures.

## *2. Theory*

Two-line atomic fluorescence (TLAF) thermometry is a ratio-metric technique, in which the temperature is derived from the ratio of the fluorescence signals from two different lower levels excited to a common upper level. For a three level electronic system with two lower states and one excited state, seen in Figure 1, two different detection schemes are commonly used. In the first detection scheme, Figure 1a, the non-resonant fluorescence is detected for each excitation. This technique is suitable in sooty and particulate laden flames as elastically scattered light can be filtered out. The major disadvantage is the need for a temperature calibration measurement to account for detector efficiencies at the different wavelengths and collection angle differences [20]. Medwell et al. have conducted measurements in the non-linear excitation regime to increase the signal-to-noise ratio with the added complexity of needing a calibration curve from a fluorescence vs irradiance plot [21]. For the second detection scheme as shown in Figure 1b, the fluorescence is detected at the same wavelength independent of the excitation wavelength obviating the need for two detectors and a

calibration measurement. Despite an increased sensitivity to elastic scattering, this has been shown to work well in low-pressure sooty flames [13].

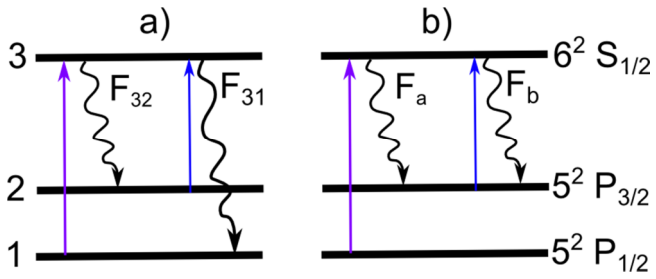


**Figure 1** Schematic of the transitions and two detection schemes used for two-line atomic fluorescence of indium. The left scheme shows detection of non-resonant fluorescence requiring two detectors while for detection scheme b) only fluorescence from level 3 to 2 is detected independent of excitation wavelength.

For a tunable light source and the detection scheme in Figure 1b, the temperature is related to the fluorescence signal, *F*, as [13]:

$$T = \frac{\Delta E/k}{\ln\left(\frac{\int F_a/I_{31}d\nu}{\int F_b/I_{32}d\nu}\right)+3\cdot\ln\left(\frac{\lambda_{32}}{\lambda_{31}}\right)+\ln\left(\frac{A_{32}}{A_{31}}\right)} \qquad (1)$$

where $\Delta E$ is the energy splitting between the two ground states, $k$ is the Boltzmann constant, $I$ the laser power, $A$ is the Einstein and ν the laser frequency. The numerical subscripts denote the transitions according to Figure 1.

The two dominant broadening mechanisms that have to be accounted for when fitting the line shapes are the Doppler broadening and the pressure broadening, also known as collisional broadening. The Doppler broadening is due to thermal molecular motion and gives rise to a Gaussian profile. The collisional broadening is more complex and arises from the interaction between an emitting molecule and the collisional species and is thus dependent on temperature and pressure, as well as local gas composition.

To analytically express the collisional broadening requires information about the local species concentrations, temperature and pressure as well as information of the reference broadening parameters for each species, which except for nitrogen and the noble gases are

unknown. The collisional broadening can be approximated using impact broadening theory and from this the FWHM of the Lorentzian can be described as [22]:

$$\Delta\nu_L = \Delta\nu_L^{ref} \left(\frac{T_{ref}}{T}\right)^{0.7} \cdot \left(\frac{p}{p_{ref}}\right) \qquad (2)$$

where a reference collisional broadening at a known temperature and pressure can be used to calculate the Lorentzian profile at other pressures and temperatures if the gas compositions remains the same. The impact broadening approximation assumes that the duration of collisions are much shorter than the time between collisions. For pressures of 50 mbar, relevant for this work, the mean free path is approximately 20 μm at flame temperatures, magnitudes greater than the atomic diameter, as needed for the impact approximation to be valid. The observed spectral line shapes will be a convolution of the Gaussian and Lorentzian profile, known as Voigt profile. If the collisional broadening is known the temperature information can be extracted from a spectral line shape by fitting a Voigt profile to the line shape using the temperature as a fitting parameter.

## *3. Experimental*

The experimental setup is shown in Figure 2. Two external cavity diode lasers, ECDL, (Toptica, DL100pro and DL100) were used to probe the two indium transitions $5^2P_{1/2} \rightarrow 6^2S_{1/2}$ and $5^2P_{3/2} \rightarrow 6^2S_{1/2}$ at 410 and 451 nm. The lasers had a power of 5 mW and were wavelength modulated to scan the hyperfine structure of each transition. Using a dichroic mirror the two lasers were spatially overlapped and sheet forming optics were employed to produce a 4 mm high laser sheet, thickness 0.2 mm, focused over the burner. A chopper wheel rotating at 10 Hz alternated between the lasers in synchronicity with the laser wavelength scanning. A reflection of the laser beam from a flat glass plate was directed to a high-finesse confocal Fabry-Perot etalon (Toptica, FPI 100) to measure the relative frequency when tuning the lasers and to ensure that the wavelength scans were mode-hop free. Two

photodiodes, before and after the flame, measured the laser power during a scan and recorded the amount of absorption of the lasers, respectively.

Perpendicular to the incident laser sheet an intensified high-speed camera (Photron, SA-X) recorded the laser-induced fluorescence signal. Wavelength scans were performed with each laser sequentially and fluorescence spectra were thus acquired at each pixel of the high-speed camera. An interference filter centred at $\lambda$=450 nm and $\Delta\lambda$±10 nm was used to reduce background chemiluminescence and detect fluorescence from the excited state to the upper level of the spin-orbit split ground state as this transition has approximately two times stronger transition cross-section than the transition to the lower ground state. The camera was mounted with an objective f# = 1.4 and imaging of a 1951 USAF resolution test card and applying the Rayleigh criterion resulted in a spatial resolution of 210 µm and a pixel size corresponding to 70x70 µm$^2$. A power meter (Thorlabs S110) was used to calibrate the power measured on the photodiode before the flame.

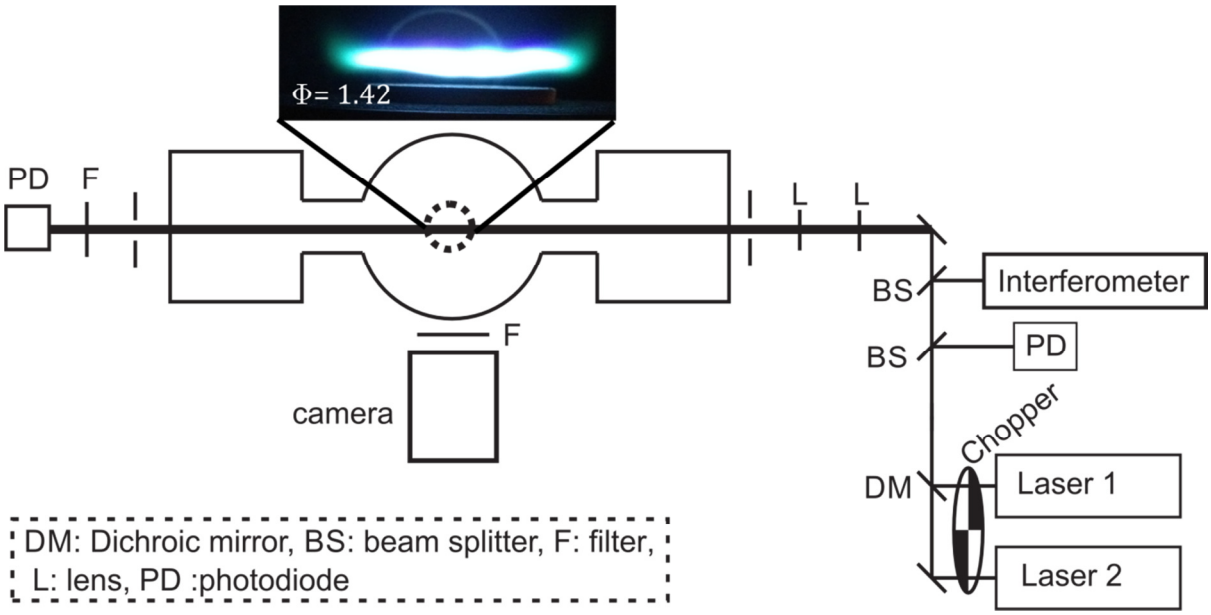


**Figure 2.** A schematic of the experimental setup. The chopper is running at 10 Hz, alternating between the scanning lasers. A PD after the burner measures the absorption of the beam and is used for adjusting the seeding concentration so as to avoid too high concentrations. PD before the flame measures the relative power of the lasers calibrated by a power meter. Inset: picture of a flame with equivalence ratio 1.42 as used in this experimental work.

The thermometry measurements were conducted on a McKenna burner with a diameter of 30 mm fitted in a low pressure chamber. A co-flow of $N_2$ prevented entrainment of ambient gases and through a translation stage the burner was adjustable in height. Mass flow controllers regulated the flow of methane, oxygen and nitrogen to the burner and the pressure of the chamber was stabilized to 50 mbar with a rotary vacuum pump. Conditions of the three flames are listed in Table 1. For richer flames $N_2$ was decreased in relation to $O_2$ to prevent blow-off. The flame conditions investigated in this paper are targeted for further study by other measurement techniques such as infra-red polarization spectroscopy [23] for modelling purposes and the temperature measurements are crucial for the wider efforts to characterize these flames.

Table I. Flame conditions. The flow is given in standard litre per minute.

| φ | $CH_4$ [SLM] | $O_2$ [SLM] | $N_2$ [SLM] | TMIn carrying gas flow [SLM] | Total flow [SLM] |
|---|---|---|---|---|---|
| 1.16 | 0.46 | 0.78 | 0.95 | 0.03 | 2.22 |
| 1.42 | 0.55 | 0.77 | 0.76 | 0.03 | 2.10 |
| 1.68 | 0.70 | 0.84 | 0.31 | 0.03 | 1.88 |

A newly developed indium seeding system was used to deliver indium atoms to the flame [15]. The working principle of the seeding system is as follows. A flow of inert gas is passed through a bubbler filled with crystallized trimethylindium (TMIn). The inert gas acts as a carrier of TMIn, where the bubbler temperature, controlled with a thermalized bath, determines the vapour pressure and thus the concentration of TMIn in the flow. The TMIn thermally decomposes when heated to produce free indium atoms. The carrier gas is mixed with the unburned gases to introduce TMIn to the combustion environment. As only a small amount of carrier gas is needed for a sufficiently high concentration of indium in the flame it is reasonable to assume that the added constituents to the flame have negligible effects on the flame properties. The investigated flames had a total flow of approximately 2 L/min whereas the TMIn flow was 0.03 L/min consisting mostly of $N_2$ carrier gas. The TMIn seeding level

was adjusted to achieve strong LIF signals while ensuring that the high concentration did not affect the temperature measurement. Detection of the fluorescence to the same level, as shown in Figure 1b, circumvents problems with self-absorption at high seeding concentrations. Instead these measurements may suffer from line-shape distortions if the concentrations are too high.

Scanning the lasers with 20 Hz a recording was made during one second with a frame rate of 6 kHz. The single-mode scanning range was 20 GHz for the $5^2P_{1/2} \rightarrow 6^2S_{1/2}$ transition and 15 GHz for the $5^2P_{3/2} \rightarrow 6^2S_{1/2}$transition. At every measurement height each pixel had an excitation scan of the two transitions averaged over ten scans, each scan consisting of 300 data points. A flat-field correction for differences in beam profile between the two lasers was made by measuring the fluorescence of the beam sheets at the highest position in the flame, where it was assumed that the temperature was uniform, and extracting a beam profile for each laser. The extracted profiles agreed well with the profiles acquired from a beam profiler allowing the use of the beam profiles measured from the indium fluorescence for flat-field corrections.

## *4. Results*

Typical normalized excitation scans of the two transitions for a single pixel are presented in Figure 3. Wavelength tuning of the lasers is accompanied by an intensity modulation that is corrected for by the base line recorded with the reference photodiode. A least-squares fitting routine is adapted to fit the measurement data to the well-known hyperfine structure of indium [24]. Voigt profiles for each of the hyperfine transitions are simulated and the complete line shape is achieved after summation of the separate profiles. To account for a non-linear frequency response in the laser tuning a quadratic polynomial is fitted to the peaks of the etalon trace. A peak signal-to-noise ratio (SNR) of 60 was achieved evaluated by

dividing the peak value by the standard deviation of the residual. Almost background free measurements are observed for the line shapes indicated by both the fitting parameter and the observable line shape seen in figure 3 when the laser is off the absorption line.

The two-line atomic temperature is insensitive to the collisional broadening due to the low pressure which allows for a two-step iterative fitting scheme to be employed to calculate the reference collisional broadening, increasing the precision of the TLAF measurement. In the first step, the temperature is calculated from Equation 1 after fitting the two-line shapes with the floating parameters temperature, background and amplitude. In the second fitting step the previously floating parameters are locked and only the reference collisional broadening is fitted. The fitted broadening parameter is used in the next iteration and after typically three iterations the temperature and broadening parameter has converged. The temperatures obtained from the line shape fits, the OLAF temperature, are in this iterative scheme locked to the TLAF temperature. As seen in Figure 3 a good agreement between the fits and the measured line shapes is achieved. The good agreement between the experimental and simulated line shapes indicates that the indium concentration is low enough so as to not distort the line shapes.

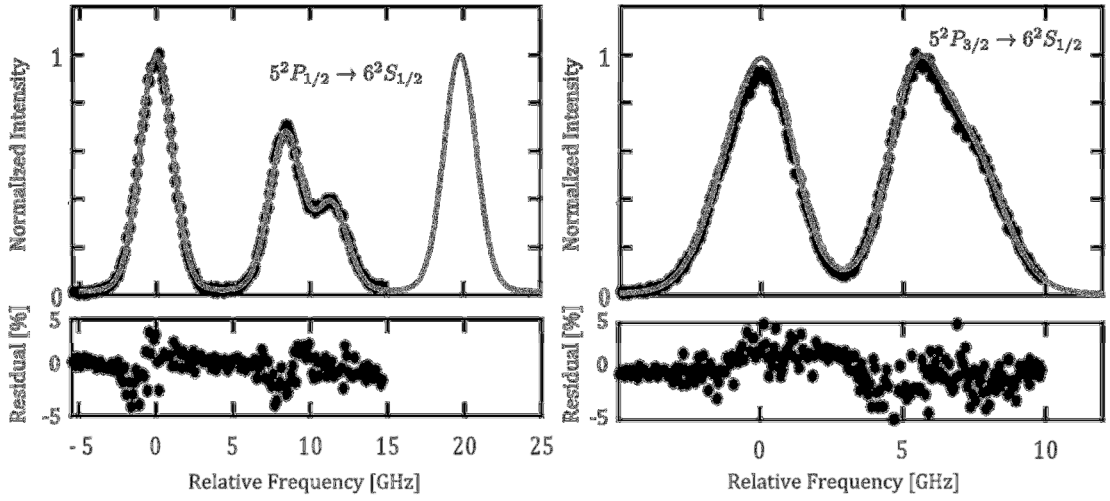

**Figure 3** *Dots* - typical recorded line shapes for a single pixel of the two lasers normalized to its maximum value. Every dot corresponds to a single frame in the recording. *Grey line* - least-square fit for the presented data. The complete hyperfine structure was not scanned due to limited single-mode scanning range of the lasers.

Two dimensional TLAF temperature maps of the three flames are shown in Figure 4 with corresponding temperature profiles along a single pixel line in the centre of the burner plotted to the right. As expected, the temperature profiles show a steep gradient in the reaction zone followed by a plateau at high temperature in the burnt gas region. The temperatures of the flames were simulated with CHEMKIN using the GRI 3.0 mechanism under the assumption of a burner stabilised flame and the result is plotted as the lines in the temperature profile plots. The TLAF temperature is observed to consistently have a lower temperature than the simulations attributed to heat losses not included in the model. For $\Phi$=1.16 and $\Phi$=1.42 the experimental temperature is approximately 120 K lower than the simulations and for $\Phi$=1.68 the difference is 60 K.

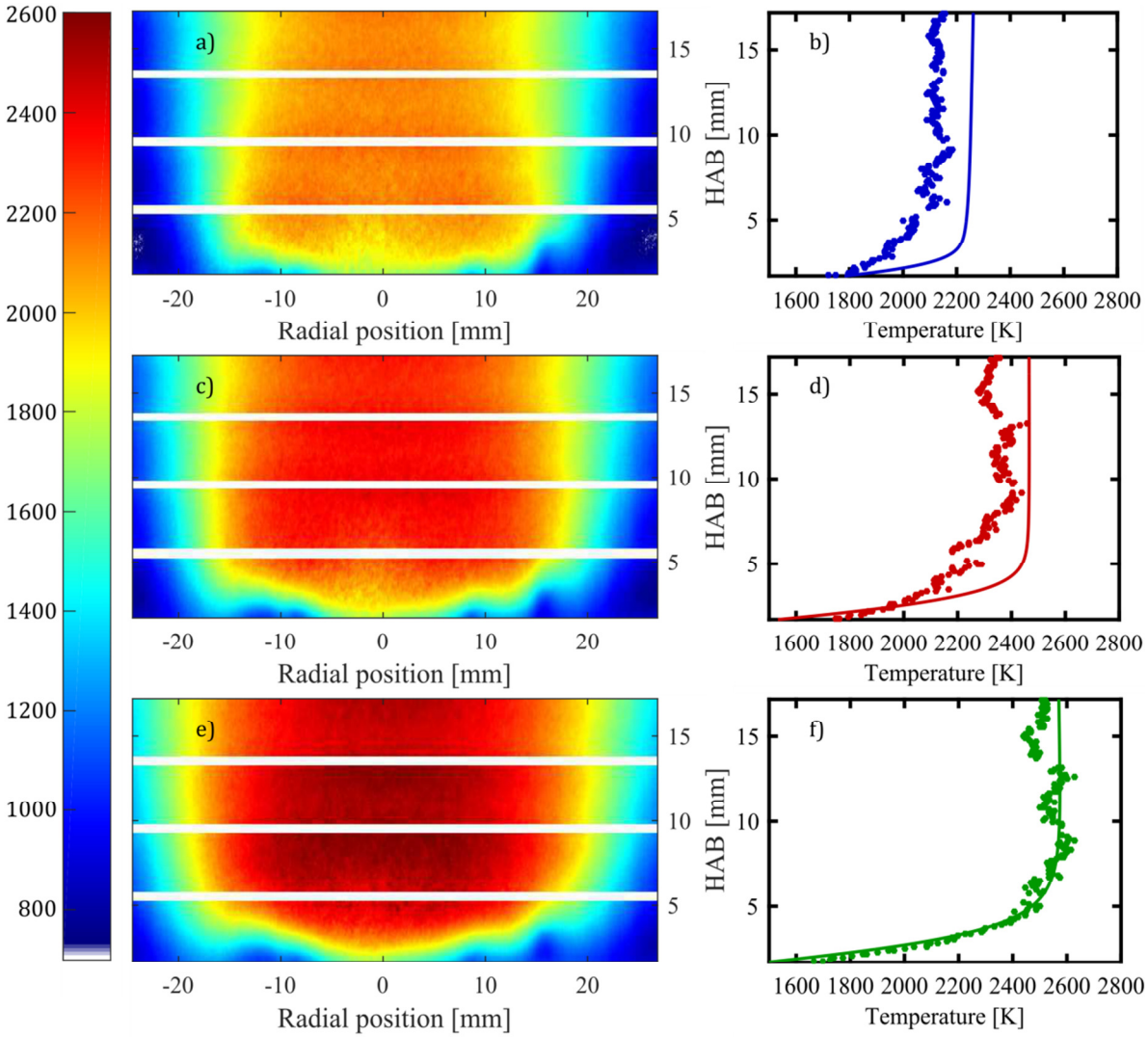


**Figure 4** To the left, TLAF temperature maps of the three flame conditions, a) Φ=1.16 c) Φ=1.42 and e) Φ=1.68. Right figures are the temperature profiles in the centre of the burner for the three flame conditions. Coloured dots correspond to the evaluated TLAF temperatures and lines are the simulated temperature profiles using CHEMKIN GRI 3.0.

The precision of the TLAF measurements is 0.7% calculated as the standard deviation in a region of the flame with a uniform temperature distribution, in this case using a box at 13 mm height above burner (HAB) with dimensions 9 pixels in the vertical direction and 60 pixels in the radial direction in the centre of the burner. An increased temperature is observed for the richer flames which, as explained previously, is due to the lower relative concentration of $N_2$ in the $O_2$-$N_2$ gas mix for these flames.

An estimated accuracy based on the error sources is presented here. The evaluated TLAF temperature is dependent on the relative power response of the power meter for the two wavelengths, 410 and 450 nm. A reasonable assumption of a relative error of 5% for the power calibration results in an error of the TLAF temperature by 3%. A more accurate power meter, such as a thermopile based power meter, would drastically increase the accuracy [13] and the error given here is not a fundamental limitation of the technique. Other notable error sources are, as previously mentioned, the reference collisional broadening, beam profile compensation and the goodness of the fit. The error of the beam profile compensation results in the slight distortions in the vertical temperature profile which is otherwise expected to be smooth. Assuming the errors are independent and normally distributed the accuracy of the technique can be estimated as the square root of the sum of squares and is for this measurement 4%.

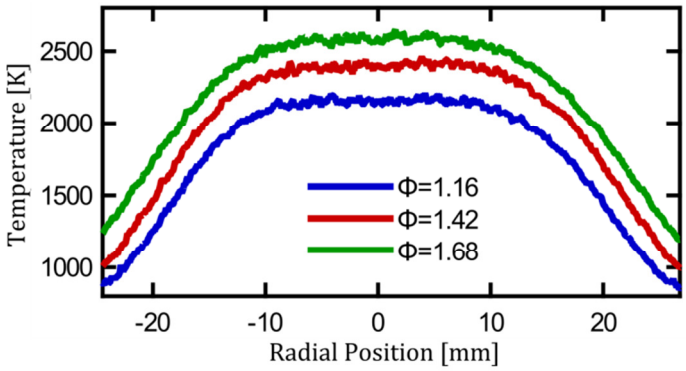


**Figure 5** Temperature cross-sections along a single pixel line at 10 mm HAB. A flat temperature profile is observed between -10 mm and 10 mm.

The horizontal temperature profile for a single pixel line at a height of 10 mm above the burner surface is shown in Figure 5. The flat flame nature of the porous plug burner holds true between -10 mm and 10 mm in the radial direction the flame thereafter a temperature decrease is seen due to the entrainment of cold co-flow gas. The smoothness of the radial cross-section is seen as an indication of the robustness of the fitting model.

The concentration of indium atoms in the flame is determined from the recorded absorption profile by the photodiode located after the flame. The recorded transmission through the flame is seen in Figure 6 as well as the best fit to the recorded data. According to the Beer-Lambert law the transmitted intensity I is related to the concentration N as

$$I = I_0 e^{-\sigma LN} \qquad (3)$$

where σ is the absorption cross-section, L the length and $I_0$ the intensity before the flame. The absorption length L is measured from the recorded LIF images and the ratio $I/I_0$ is the resulting transmission presented in Figure 6. The absorption cross-section is calculated from the Einstein A coefficient.

$$\sigma(\nu) = \frac{A\lambda^2 \phi(\upsilon - \nu_0)}{8\pi} \frac{g_n}{g_m} \qquad (4)$$

Here $\lambda$ is the wavelength of the transition, $\phi$ is the normalized line shape function and the $g_n$ and $g_m$ are the degeneracies of the upper and lower states respectively. Integration over the line shape for both the cross-section expression and absorbance data and applying equations 3 and 4 yields a concentration of 0.27 ppm indium in the flame. This is a substantial fractional absorption but a fairly high seeding concentration was chosen in order to demonstrate the principal of diode laser TLAF imaging. For axis-symmetric flames like the one studied here, the effects of absorption can be compensated for by calculating the local laser power at the measurement volume. It has been shown previously that temperature measurements by the single-detector TLAF scheme are insensitive to signal trapping. Nevertheless, strong fluorescence signals are evident from the spectra shown in Figure 3, meaning that much lower seeding concentrations could be used in future to avoid any influence of laser absorption on the measured temperature. Similar concentrations as have been shown for atmospheric flames under the same seeding conditions [16].

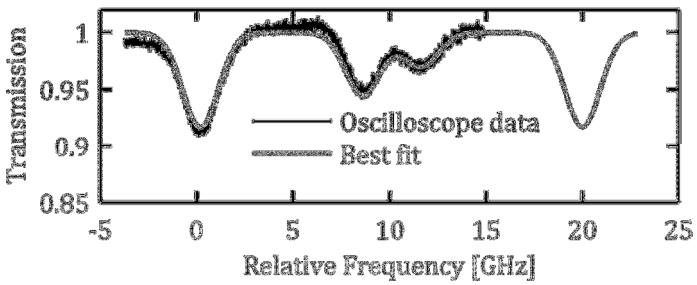


**Figure 6** Transmission of the laser tuned over the $5^2P_{1/2} \rightarrow 6^2S_{1/2}$ transition recorded on a photodiode after the flame and the best fit.

## *5. Conclusions*

In this work we have demonstrated two-dimensional imaging of flame temperature using diode lasers for the first time. Previous work on diode laser two-line atomic fluorescence was restricted to point measurements but advances in diode laser output power and camera technology have allowed mapping of the temperature field in low-pressure methane flames to provide data for validation of chemical kinetic models. This demonstration of planar laser induced fluorescence imaging with compact, inexpensive, low-power light sources is a significant step forward since such measurements have been performed in the past with high-power, pulsed dye lasers. The spectral purity of the diode lasers allows a fully-resolved indium spectrum to be recorded at every camera pixel. A novel indium seeding system providing more flexibility than conventional arrangements allowed indium seeding through a sintered porous plug McKenna type burner while avoiding the addition of water vapour to the premixed gases. Diode lasers were shown to give a peak SNR of 60 for imaging purposes, which highlights the future potential to make temperature measurements more quickly and/or at lower seeding levels than has been reported here. The accuracy of the measurements reported in this first demonstration of TLAF imaging was estimated to be ±4% at flame temperatures but this is by no means a limitation of the technique and would be drastically improved by using a laser power meter that is insensitive to wavelength. More accurate beam

profile compensation will further increase the accuracy and the precision of the technique and reduce the spread in vertical direction. These improvements may be expected to lead to measurement uncertainty similar to that previously demonstrated for single-point diode laser TLAF studies. The temperature measurements were shown to compare well to chemical kinetic simulations. Thanks to the simplicity of the setup, the technique is expected to be applicable to a wide range of other laminar flames and particularly well-suited to fuel-rich and sooting flames, including those with sharper and more complex spatial gradients than the one studied here.

## *Acknowledgements*

The work was financially supported by the Swedish Energy Agency, Swedish Research Council (VR), Knut & Alice Wallenberg Foundation and European Research Council.

1 Y. Li, L. Wei, Z. Tian, B. Yang, J. Wang, T. Zhang*, et al.*, *Combust Flame* 152, 336 (2008)
2 A. Frassoldati, R. Grana, T. Faravelli, E. Ranzi, P. Oßwald, and K. Kohse-Höinghaus, *Combust Flame* 159, 2295 (2012)
3 Z. Wang, L. Zhao, Y. Wang, H. Bian, L. Zhang, F. Zhang*, et al.*, *Combust Flame* 162, 2873 (2015)
4 U. Struckmeier, P. Oßwald, T. Kaspert, L. Bohling, M. Heusing, M. Kohler*, et al.*, *Zeitschrift fur Physikalische Chemie* 223, 503 (2009)
5 R. Dibble and R. Hollenbach, *Symposium (International) on Combustion* 18, 1489 (1981)
6 A. T. Hartlieb, B. Atakan, and K. Kohse-Höinghaus, *Appl. Phys. B* 70, 435 (2000)
7 H. Kronemayer, P. Ifeacho, C. Hecht, T. Dreier, H. Wiggers, and C. Schulz, *Appl. Phys. B* 88, 373 (2007)
8 A. Bohlin and C. J. Kliewer, *J. Phys. Chem. Lett.* 5, 1243 (2014)
9 A. Bohlin, M. Mann, B. D. Patterson, A. Dreizler, and C. J. Kliewer, *Proceedings of the Combustion Institute*
10 A. Lawitzki, I. Plath, W. Stricker, J. Bittner, U. Meier, and K. Kohse-Höinghaus, *Appl. Phys. B* 50, 513 (1990)
11 S. Li, A. Farooq, and R. K. Hanson, *Meas. Sci. Technol.* 22, 125301 (2011)
12 R. S. M. Chrystie, E. F. Nasir, and A. Farooq, *Proceedings of the Combustion Institute* 35, 3757 (2015)
13 I. S. Burns, X. Mercier, M. Wartel, R. S. M. Chrystie, J. Hult, and C. F. Kaminski, *Proceedings of the Combustion Institute* 33, 799 (2011)
14 R. S. M. Chrystie, I. S. Burns, J. Hult, and C. F. Kaminski, *Opt. Lett.* 34, 2492 (2009)
15 I. Burns, N. Lamoureux, C. Kaminski, J. Hult, and P. Desgroux, *Appl. Phys. B* 93, 907 (2008)
16 R. Whiddon, B. Zhou, J. Borggren, M. Aldén, and Z. Li, *Rev. Sci. Instrum.* 86, 093107 (2015)
17 C. A. Taatjes, N. Hansen, A. McIlroy, J. A. Miller, J. P. Senosiain, S. J. Klippenstein*, et al.*, *Science* 308, 1887 (2005)

18 Z. S. Li, C. Hu, J. Zetterberg, M. Linvin, and M. Aldén, *J. Chem. Phys.* 127, 2007)
19 Z. S. Li, M. Linvin, J. Zetterberg, J. Kiefer, and M. Aldén, *Proceedings of the Combustion Institute* 31, 817 (2007)
20 J. E. Dec and J. O. Keller, *Symposium (International) on Combustion* 21, 1737 (1988)
21 P. R. Medwell, Q. N. Chan, P. A. M. Kalt, Z. T. Alwahabi, B. B. Dally, and G. J. Nathan, *Appl. Opt.* 48, 1237 (2009)
22 I. S. Burns, J. Hult, G. Hartung, and C. F. Kaminski, *Proceedings of the Combustion Institute* 31, 775 (2007)
23 Z. S. Li, M. Rupinski, J. Zetterberg, Z. T. Alwahabi, and M. Aldén, *Chem. Phys. Lett.* 407, 243 (2005)
24 G. V. Deverall, K. W. Meissner, and G. J. Zissis, *Phys. Rev.* 91, 297 (1953)